Journal of Applied Polymer Science

Water vapor sorption and diffusion in wheat straw particles and their impact on the mass transfer properties of biocomposites

Caroline Wolf, Valérie Guillard, Hélène Angellier-Coussy, Gabriella Ghizzi D. Silva, Nathalie Gontard
UMR 1208 IATE "Agropolymers Engineering & Emerging Technologies" (INRA-UM-Montpellier SupAgro-CIRAD), Campus INRA-Montpellier SupAgro, Bât 31, 2 Place Viala, 34060 Montpellier Cedex 2, France
Correspondence to: V. Guillard (E-mail: guillard@univ-montp2.fr)

ABSTRACT: This work intends to decipher the role of hydrophilic fillers, wheat straw fibers (WSF), on the water vapor transfer properties (sorption and diffusion) of biocomposites based on poly(3-hydroxybutyrate-co-3-hydroxyvalerate), (PHBV) as matrix. Transfer in biocomposites, measured using dynamical vapor sorption measurement, is correlated to the transfer properties of each individual constituent and to the specific structural arrangements induced by the presence of particles inside the matrix. Increasing amounts of WSF particles in the PHBV matrix lead to an increase of the water vapor sorption (WVS) of the resulting composites. This is attributed to the high sorption of hydrophilic WSF as compared to that of the neat PHBV matrix. Water vapor diffusion in composites (around 0.13×10^{-11} m^2 s^{-1} at 20°C whatever the filler content) is always lower than in the neat matrix (0.26×10^{-11} m^2 s^{-1}) although wheat straw displays high diffusivity values (1.84×10^{-11} m^2 s^{-1}). Such unexpected behavior is related to (1) changes of structure and properties of the WSF particle once embedded in the PHBV matrix, (2) changes in the polymer matrix structure and properties in contact with fibers, and also (3) to the representativeness of the filler diffusivity, which is difficult to appraise. © 2016 Wiley Periodicals, Inc. J. Appl. Polym. Sci. **2016**, *133*, 43329.

KEYWORDS: biodegradable; composites; fibers; packaging; properties and characterization

Received 5 October 2015; accepted 9 December 2015
DOI: 10.1002/app.43329

INTRODUCTION

Composites are materials consisting of at least two non-miscible constituents with different properties, whose synergism creates properties unavailable from individual single constituents. Due to increasing environmental concerns, great attention has been paid, during the last decade, to the study of the manufacture, structure, and properties of biocomposites.[1] Last progresses in the domain were devoted to the production of biopolymers from food wastes and their processing in composite structure with vegetal fibers in order to decrease their overall cost and modulate their functional properties. For example, poly(3-hydroxybutyrate-co-3-hydroxyvalerate) (PHBV) is considered to be a good alternative to non-biodegradable synthetic polymers because it is an environmentally friendly material issued from renewable resources and moreover, it is biodegradable. Its production is now possible from liquid effluents from the food industry.[2–4] However, its high manufacturing costs are still hampering the market growth of this material. Vegetal fibers are attractive for their high strength, low density, wide availability throughout the world, low environmental and economic cost, and non-food origins. The incorporation of cheap fillers such as wheat straw fibers (WSF) in PHBV has already been considered to overcome the drawback of the cost[5–9] of PHBV. A potentially undesirable effect of introducing naturally hydrophilic vegetal fibers in a hydrophobic polymer matrix is the higher water sensibility of the resulting composites. On one hand, moisture transfer in the biocomposite could lead to a substantial alteration of the functional properties of the material, especially under usage conditions, due to an accelerated degradation of its constituents in the presence of water molecules,[10,11] as well as to an alteration of the fiber-matrix adhesion.[12–14] On the other hand, in the field of food packaging, fresh and respiring foods such as fruits and vegetables or cheeses need to be packed with materials presenting sufficiently high moisture and gases transfer properties.[15–19] A good knowledge of the impact of each constituent on the water transfer in vegetal fiber-based composites and especially water in its vapor form is required to design materials tailored to targeted applications. A significant number of publications have already been devoted to the study of liquid water transfer in biocomposites and constituting biopolymers and fibers.[12,20] For example, Srubar *et al.*,[12] demonstrated that the presence of hydrophilic wood fibers in composites increased both the water content at equilibrium and the identified liquid diffusion coefficient. However, in literature, transfer properties

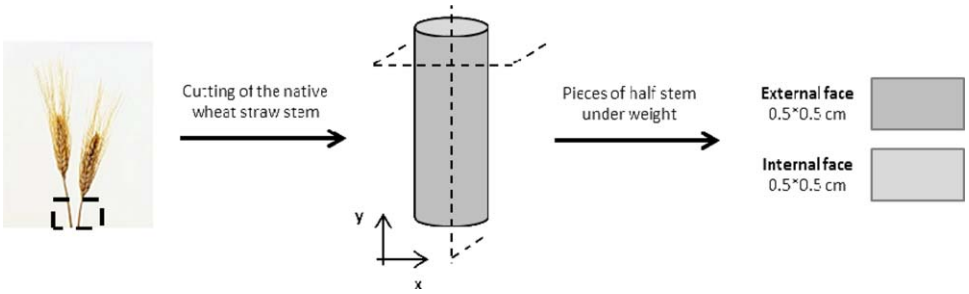

Figure 1. Explanation of the cutting procedure for the preparation of wheat straw fiber piece for DVS experiment. [Color figure can be viewed in the online issue, which is available at wileyonlinelibrary.com.]

of water in its vapor form have been very little discussed for vegetal fibers-based biocomposites. This could be related to the difficulty to evaluate the diffusivity into the fiber itself. In the aforementioned studies, diffusivity is usually obtained from water vapor sorption (WVS) measured on fiber powders or stacks. Extrapolation of this value to the diffusivity within the single particle could be questionable. It seems, therefore, indispensable to determine not only liquid diffusivity but also water vapor diffusivity.

In the framework of the European program EcoBioCap (http://www.ecobiocap.eu), a huge effort was put on the development and characterization of biocomposites made of poly(3-hydroxybutyrate-co-3-hydroxyvalerate) and ligno-cellulosic fiber for food packaging applications. Several papers of our group focusing on mechanical properties[5–7,21] and aging in real conditions[22] of use, have highlighted the role of water transfer within the material, which would be determinant for its stability. Therefore, the present study aims at deciphering water vapor transfer mechanisms in these biocomposites (PHBV/wheat straw fibers). Water vapor sorption and diffusion in biocomposites containing two different percentages of WSF were experimentally evaluated and discussed in relation to their structural and thermal characteristics and to the sorption and diffusion properties of the individual PHBV and WSF constituents. Much effort was dedicated to the experimental evaluation of the diffusion properties, which are much more difficult to address than sorption. A dedicated experiment was set up for assessing water vapor diffusivity in the wheat straw particle itself, which had never been attempted before.

EXPERIMENTAL

Materials

Commercial poly(3-hydroxybutyrate-co-3-hydroxyvalerate) (PHBV) was supplied by Tianan under the reference Y1000P with a HV content of 3 wt %. Wheat straw (*Triticum aestivum cv.* Apache) was provided by Fernand Meaux (Saint Jean du Salés, Tarn, France), harvested in 2007 and was ground at a size of 100–150 µm to obtain wheat straw fiber using a process previously developed[23] and recently re-used.[6,7] Wheat straw was composed of $32.0 \pm 0.7\%$ cellulose, $20.5 \pm 0.4\%$ hemicelluloses (arabinoxylans), $17.4 \pm 0.3\%$ Klason lignin, $9.5 \pm 2.2\%$ extractives, and $6.1 \pm 0.1\%$ dry wheat straw, with a moisture content of 8% (w.b.).[23]

Preparation of the PHBV and Composite Films

PHBV and PHBV/WSF compounds containing 10 wt % and 20 wt % of WSF (PHBV/10WSF and PHBV/20WSF) were prepared by extrusion using a lab-scale twin-screw extruder with an L/D = 40 and a screw diameter of 16 mm (Eurolab from ThermoFisher Scientific) using a procedure previously described.[7] In short, polymer pellets and wheat straw fiber were delivered at a total rate of 1 kg h^{-1}. The temperature profile from the polymer feeding to the die varied from 180°C to 160°C. A rod die with a 3 mm diameter was adapted at the end of the barrel and the obtained solid string was then pelletized. Before extrusion, virgin PHBV pellets and wheat straw fiber were dried in an oven at 60°C for at least 8 hours. After extrusion, the resulting compounds were dried in the same conditions and then kept in sealed plastic bags containing a desiccant.

Composite films (about 15 × 15 cm) were obtained by thermopressing using a heated hydraulic press (PLM 10 T, Techmo, Nazelles, France) during 5 minutes at 170°C and 0 bar and then 5 min at 170°C and 150 bar as previously used by Berthet *et al.*[7]

Sample Preparation and Conditioning before Water Vapor Sorption Measurement

PHBV and PHBV/WSF composite films were respectively cut into discs of 0.8 cm diameter and stored on P_2O_5 at room temperature for 10 days before their use. Native wheat straw internode was prepared with a first perpendicular cut to its height in order to obtain a cylinder, which was in turn itself cut vertically down the middle. The cut was then easily flattened into a square piece of approximately 0.5 × 0.5 cm^2 by putting it under weight pressure at around 200 N m^{-2} during one week (Figure 1).

Characterization of the WSF, PHBV, and Composites

The apparent density was calculated from the ratio of the dry matter weight to the volume of total material. The thickness of the films was measured using a micrometer (Braive Instruments, Chécy, France).

The true weight (w) and volume (φ) fractions of particles were determined by ash content analysis performed using a Thermolyse 6000 device from a furnace at 550°C during 2 hours on samples with a mass in the range between 2 g and 5 g. Then, the quartz incineration pans were put in a desiccator at room temperature under dry $CaCl_2$ during 30 minutes before being weighed; w was calculated from the inorganic residue:

$$w = \frac{R_{PHBV/WSF} - R_{PHBV}}{R_{WSF} - R_{PHBV}} \quad (1)$$

where $R_{PHBV/WSF}$, R_{PHBV}, and R_{WSF} are the inorganic residue of the PHBV/WSF composites, PHBV and WSF. And then, φ was calculated with the following equation:

$$\varphi = \frac{\frac{w}{\rho_{WSF}}}{\frac{w}{\rho_{WSF}} + \frac{1-w}{\rho_{PHBV}}} \quad (2)$$

where ρ_{WSF} and ρ_{PHBV} are the WSF and PHBV density, respectively, and w the true weight fraction of WSF previously measured.

Differential scanning calorimetry (DSC) measurements were performed using a thermo-modulated calorimeter (Q200 modulated DSC, TA Instruments, New Castle). The samples, with a mass ranging from 6 mg to 9 mg, were placed in open aluminum pans, which were immediately hermetically sealed. Samples were first heated from 40°C to 190°C with a ramp rate of 50°C min^{-1}. The samples were then cooled with a cooling rate of 10°C min^{-1} down to −40°C and after heated with a heating rate of 10°C min^{-1} to 190°C using N_2 as purging gas. The crystallinity of the PHBV was calculated with the following equations:

$$\chi_c = \frac{\Delta H_f(PHBV)}{\Delta H^0(PHBV)} * \frac{100}{w_{PHBV}} \quad (3)$$

where ΔH^0(PHBV) is the melting enthalpy per gram of 100% crystalline (146 J g^{-1})[24] and w_{PHBV} the weight fraction of PHBV in the composite.

Microscopic Observations

WSF internodes and nodes were humidified for two days at 4°C with deionized water under vacuum in a desiccator. About 50 and 100 μm thick transverse sections were prepared with a vibratome Microcut H1200 (Bio-Rad, UK). These fresh sections were observed in a stereomicroscope MVX 10 (Olympus, JP) equipped to observe fluorescence (Optical objective ×1.6, optical zooms ×1 and ×2).

Optical microscopy observations of PHBV/20WSF cross-sections were performed on thin samples (cuts of approximately 3 μm thick) obtained after the cut with a microtome of composite samples previously embedded in Technovit® hydroxyethylmethacrylate resin. A Leica MacroFluo Leica Z6 APO 16:1 was used for the observations.

Moisture Sorption Kinetics of WSF, PHBV and Composites

Water vapor sorption (WVS) experiments were carried out at 20°C over a range of relative humidity from 0 to 95 using a controlled atmosphere microbalance apparatus (DVS, Dynamical Vapor Sorption system, Surface Measurement System, London, UK) described in a previous publication.[25] The samples were first re-equilibrated at 0% relative humidity for a time frame of 24 hours to establish a dry mass (M_d) and then exposed to different levels of relative humidity by a continuous air stream of a specific relative humidity. Mass equilibrium was reached at each humidity level by measuring the percent of mass change with respect to time ($dm/dt < 0.002$) for WSF. The values of water content at each equilibrium (X) were used to build the sorption isotherm:

$$X = \frac{M_w - M_d}{M_d} \quad (4)$$

where M_w (g) is the mass of wet sample at equilibrium state and M_d (g) the dry mass.

Modeling of Water Vapor Sorption Isotherm

Sorption Models. Several models are available in literature for the description of WVS.[26] Among them, Guggenheim, Anderson and de Boer (GAB) and Park models have turned out to be the most useful for the fitting of water vapor sorption data for carbohydrate materials, food materials, and biopolymer films. Moreover, their adjustable parameters have a physical meaning, which is not always the case for other mathematical representations of the water sorption curves. They have thus been selected in this study for modeling water sorption curves of wheat straw, PHBV, and resulting biocomposites. GAB model considers that water molecules condense layer by layer on adsorption surfaces such as external surfaces, specific sites or internal surfaces of cavities or pores:

$$X = \frac{X_m \cdot C_g \cdot K \cdot a_w}{(1 - K \cdot a_w)(1 - K \cdot a_w 1 + C_g \cdot K \cdot a_w)} \quad (5)$$

where X is the water content at equilibrium as calculated by eq. (4), X_m is the monolayer of water content, C_g the Guggenheim constant, and K the constant relative to the adsorption energies of second and subsequent layers, which lie somewhere between the monolayer adsorption energy and the pure adsorptive liquefaction energy.[27]

Park model corresponds to a multi-sorption model (succession of Langmuir, Henry-type, and water clustering modes), which could be divided into three steps. The corresponding equation can be written as follows:

$$X = \frac{A_L \cdot b_L \cdot a_w}{1 + b_L \cdot a_w} + k_H \cdot a_w + K_a \cdot a_w^n \quad (6)$$

with A_L the Langmuir capacity constant, b_L the Langmuir affinity constant, k_H the Henry's solubility coefficient, K_a the equilibrium constant for the clustering reaction, and n the mean number of water molecules per cluster.

Models were fitted to water vapor isotherm using the GRG nonlinear solver from Excel 2010. In order to evaluate the fit of each model to the experimental data, the regression coefficient (R^2) and mean relative percentage of deviation modulus (E) were determined; a modulus value below 10% was usually an indicator for a good fit.[28]

Water interactions in WSF, PHBV, and Composites. Zimm and Lundberg theory,[29] based on statistical mechanics, have developed a theory to determine the degree of clustering defined under the clustering function which is defined as the ratio of the clustering integral ($G_{w,w}$) to the partial molecular volume of water (V_w) and was calculated from the equation of the water vapor sorption isotherm.

$$\frac{G_{w,w}}{V_w} = -(1 - \Phi_w)\left[\frac{\partial\left(\frac{a_w}{\Phi_w}\right)}{\partial a_w}\right] - 1 \quad (7)$$

where Φ_w and a_w are the water volume fraction and activity. In their theory, the mean cluster size has been defined as:

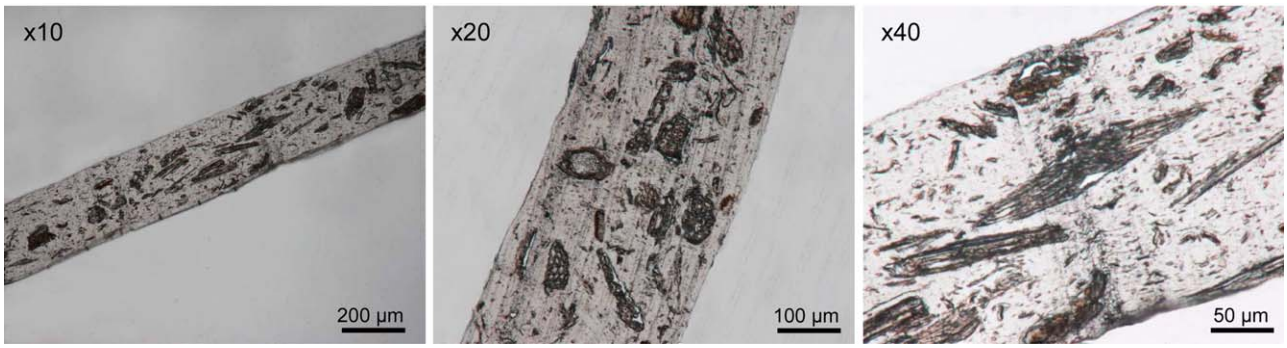

Figure 2. Optical microscopy observations of the cross section of the composite material PHBV20 at magnification 10, 20, and 40. [Color figure can be viewed in the online issue, which is available at wileyonlinelibrary.com.]

$$MCS = 1 + \frac{\Phi_w G_{w,w}}{V_w} \quad (8)$$

engaged species induced clustering model (ENSIC) model,[30] based on a probabilistic and mechanistic approach, has been developed in order to describe different types of molecular interactions in solvent-polymer systems. The model considers the probability of insertion of one molecule in a polymer matrix containing only the polymer and previously sorbed molecules. The increase of sorbed solvent molecule number (dn_s) due to an increase of the pressure (dP) in the gaseous phase can be related as:

$$dn_s = (k_p n_p + k_s n_s)\left(\frac{dP}{P_0}\right) \quad (9)$$

where n_s and n_p represent the solvent and the polymer cell numbers in the polymer, and k_p and k_s the affinity between the non-polymeric molecule and the polymer or the previously sorbed molecules respectively. Assuming the gas phase as ideal, integration of eq. (9) leads to the following expression:

$$\Phi_w = \frac{e^{(k_s - k_p)\cdot a_w} - 1}{(k_s - k_p)/k_p} \quad (10)$$

where Φ_w and a_w are the water volume fraction and activity.

Effective Moisture Diffusivity Identification in WSF, PHBV, and Composites

Effective moisture diffusivity (D_{eff}) values at different water activities were identified from moisture sorption kinetics measured using the dynamical vapor sorption (DVS) apparatus. The material samples, in the form of flat films, used in the DVS apparatus were thin enough for the water vapor diffusion to be considered as one-dimensional in the axial direction. The procedure, used in this study for the identification of D_{eff}, was the same than that developed and presented by Guillard *et al.*,[25] and successfully applied to starch based-films[31] and to wheat gluten-based films.[32] The moisture sorption kinetic within the samples, assuming that the film did not swell, that the diffusivity coefficient remained constant for a given water activity stage, that the flux was equal to zero at the lower face of the sample in contact with the holder, and that the film upper surface was instantaneously equilibrated at the surrounding a_w, could be modeled using the following equation[33]:

$$\frac{M_t}{M_\infty} = 1 - \sum_{n=0}^{\infty} \frac{8}{(2n+1)^2 \pi^2} \exp\left(\frac{-D_{eff}(2n+1)^2 \pi^2 t}{4l^2}\right) \quad (11)$$

where M_t (g g(dry basis)$^{-1}$) denotes the total amount of water vapor which has entered the film at time t, M_∞ (g g(dry basis)$^{-1}$) the quantity of water vapor content after an infinite time, and l the film thickness (m).

RESULTS AND DISCUSSION

Impact of WSF Particles on the Multi-Scale Structure of Biocomposites

Following successive dry grinding steps (cut milling and impact milling) of native straw, wheat straw fibers displayed a size of about 62 μm, corresponding to the median value of the area-based distribution of equivalent diameters.[34] They were characterized by a high polydispersity and heterogeneity in terms of size, shape, density, and surface aspect, as revealed in a preliminary work by laser granulometry coupled with statistical image analysis of light microscopic observations.[7] A broad size distribution (sizes ranging from the order of the millimetre down to few microns) in the case of thin ones (called "fines") was induced by grinding. It was related to the complex heterogeneous structure of wheat straw, especially in terms of histological tissues and anatomic parts of the plant, that break in different size depending on the resistance of the tissue. The particle aspect ratio was approximated by the elongation parameter (defined as the maximum dimension inside the particle projection divided by the equivalent short rectangle side) obtained on area-based distributions and was equal to 2.3.[34] Light microscopic observations of thin cuts of biocomposites allowed us to confirm the *in situ* ellipsoidal shape of ground WSF as well as the heterogeneity in terms of size (both coarse and fine (dust) particles in the sample) and shape (more or less elongated or round) (Figure 2).

Light microscopic observations (Figure 2) have also highlighted that wheat straw fibers were well embedded by the polymer matrix but tended not to be homogeneously distributed within the thickness of the films: biggest WSF particles seemed to be preferentially in the core of the film, whereas, fine ones were distributed more homogeneously. Smaller particles more tended to create aggregates, especially due to the fact that the fiber/matrix affinity is lower than fiber/fiber affinity. As regards the orientation, materials were almost isotropic due to the low

Table I. Density, Particle Fraction, Crystallization (Tc) and Melting (Tm) Temperatures, Melting (ΔH_m) Enthalpy, and Crystallinity (χ_C) Calculated from DSC Results of PHBV Films and Biocomposites, Containing WSF Particles

Sample	Density ($g.cm^{-3}$) Experimental density	Particle fraction (%)		Crystallinity			
		Weight fraction	Volume fraction	T_m (°C)[a]	T_c (°C)[a]	ΔH_m ($J\ g^{-1}$)	χ_C (%)
PHBV	1.12 ± 0.01			172.8	122.5	101.67 ± 0.87	69.6 ± 0.6
WSF	1.69 ± 0.03[b]						
PHBV/10WSF	1.13 ± 0.03	7.58 ± 1.44	5.14 ± 0.98	171.4	118.6	92.05 ± 0.24	68.2 ± 0.2
PHBV/20WSF	1.16 ± 0.02	16.30 ± 1.69	11.40 ± 1.20	168.8	116.1	81.21 ± 0.54	66.4 ± 0.4

[a] Standard error of +/-0.5°C.
[b] From Ref. 10.

aspect ratio of particles. It is worth noting that the most elongated particles were logically preferentially oriented parallel to the surface of the film (Figure 2). Finally, preliminary works have demonstrated using scanning electron microscopy (SEM) analysis of film cross-sections a poor adhesion at the particle/matrix interface, which was revealed by the presence of fiber pull-outs and interfacial gaps.[7] These interfacial gaps are also visible on light microscopic scans (Figure 2). The aforementioned features highlighted that composites displayed a quite good mixing phase, but also some heterogeneities and defects at the microscopic scale that could influence their moisture transfer properties (especially diffusivity), by inducing preferential pathways.

The introduction of fibers is also known to affect inherent properties of the matrix, such as molecular weight or crystallinity, which could themselves have an effect on functional properties. DSC analysis enabled to assess thermal behavior as well as crystallinity of materials (Table I). The melting temperature significantly decreased for composites confirming polymer degradation during process triggered by the presence of WSF. A slight but significant decrease of the temperature of crystallization was induced by the presence of wheat straw fibers, implying that crystallization and implicitly polymer chain mobility was hindered by fibers. As regards crystallinity approximated by DSC, it decreased slightly, which was coherent with the previously supposed decrease in polymer chain mobility.

Water Vapor Sorption Isotherms of WSF, PHBV, and Biocomposites

Water vapor isotherms of WSF and PHBV films [Figure 3(a)] highlighted that the individual WSF piece was more hydrophilic than PHBV films. At a water activity equal to 0.95 (i.e., 95% relative humidity), the water content in the WSF piece was approximately 36 times as high as PHBV films. Water vapor isotherm results were coherent with previous published results on moisture sorption of PHBV.[7,35] Miguel and Iruin[35] found in PHBV (8% HV), at 30°C, a moisture content of 3.5×10^{-3} g $g^{-1}_{(drybasis)}$ at 50% RH and 7.0×10^{-3} g $g^{-1}_{(drybasis)}$ at 95% RH, against $2.05 \pm 0.47 \times 10^{-3}$ and $5.43 \pm 1.05 \times 10^{-3}$ g $g^{-1}_{(drybasis)}$ for our PHBV (3% HV) at the same RH but at a temperature of 20°C. Berthet *et al.*,[7] found similar values of water sorption on PHBV (3% HV) at 20°C. All aforementioned studies (included this work) showed that moisture sorption as function of relative humidity of PHBV film was almost linear until 80% RH and then exhibited a slightly higher slope at higher a_w.

As regard wheat straw [Figure 3(a)], the water vapor isotherm of the cut piece of wheat straw displayed a sigmoidal evolution characteristic of hydrophilic materials and corresponding to type II of the sorption modes from Brunauer classification.[36] Similar water sorption isotherms were obtained for the powder of ground WSF. An average water sorption isotherm was then

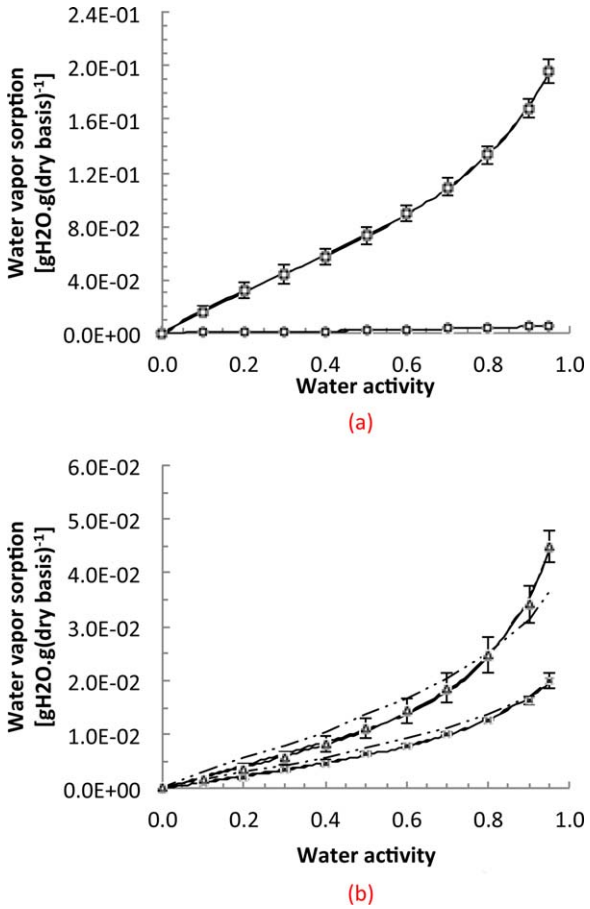

Figure 3. Water vapor sorption isotherms of (a) PHBV (circle) and WSF (square) with prediction by eq. (5) for PHBV and eq. (6) for WSF (solid lines), and (b) water vapor sorption isotherm of PHBV/10WSF (cross) and PHBV/20WSF (triangle) with prediction of eq. (6) for PHBV/10WSF and PHBV/20WSF (solid lines), and prediction of the rule of mixture (dotted lines). [Color figure can be viewed in the online issue, which is available at wileyonlinelibrary.com.]

Table II. GAB and Park Fitting Parameters Which Were Identified from the Water Vapor Sorption Isotherm of PHBV, WSF, and PHBV/WSF Composites at 20°C

	GAB parameters					Park parameters						
Samples	X_m	C_g	K	R^2	E (%)	A_L	b_L	k_H	K_a	n	R^2	E (%)
PHBV	0.004	1.388	0.571	0.999	2.26	0.033	0.034	0.002	0.003	3.262	0.998	2.85
WSF	0.065	4.090	0.736	1.000	1.37	0.259	0.345	0.068	0.091	6.151	1.000	1.78
PHBV/10WSF	0.007	2.227	0.748	0.998	4.63	0.068	0.070	0.007	0.011	5.026	0.998	6.50
PHBV/20WSF	0.009	2.652	0.850	0.999	4.76	0.079	0.083	0.015	0.034	6.714	0.997	7.87

calculated from results obtained on ground WSF and those obtained for the piece of wheat straw. This shape characteristic of a hydrophilic material was already presented in previous publications from the literature for different fibers of various botanical species, i.e., agave fibers,[37] cellulose whisker,[38] flax fibers,[39,40] and could be described as multi-stages sorption.

Our results reflect the hydrophilic character of WSF due to hydroxyl groups of cellulose. We can anticipate that the WSF will fully participate in the general moisture sorption process of biocomposites since PHBV displayed, in comparison, very low water sorption.

Confirming this, water vapor isotherms of biocomposites [Figure 3(b)] displayed the same sigmoid shape as WSF with nevertheless less pronounced upturns at higher a_w. The major role played by WSF on the increase of water sorption of biocomposites compared to neat PHBV was even more pronounced for PHBV/20WSF than PHBV/10WSF. Previous published data on water vapor sorption of composites containing fibers were obtained on nanocomposite materials containing cellulose nanowhiskers, which is a completely different system. Comparison of these previous data with our data was, thus, not attempted. In order to further understand the contribution of each constituent, the rule of mixtures [eq. (12)] was applied to predict water vapor sorption in the composites:

$$X_{PHBV/WSF} = W_{WSF}X_{WSF} + W_{PHBV}X_{PHBV} \quad (12)$$

where $X_{PHBV/WSF}$ is the water vapor content in the biocomposites, W_{WSF} and W_{PHBV} the weight fraction of WSF and PHBV, and X_{WSF} and X_{PHBV} the water vapor content of WSF and PHBV at each a_w; resulting plots were illustrated in Figure 3(b) for both composites (dotted lines). In a general way, the rule of mixture permitted to approximate the water vapor sorption of the composite but most often overestimated it. For PHBV/20WSF, a discrepancy between the shape of calculated and experimental curves is observed with an overestimation of water vapor at RH lower than 80% and an underestimation for higher RH. The rule of mixture failed on representing the sigmoidal part of the sorption isotherm at high RH. The water vapor sorption behavior of composites can be concluded to not result from a simple addition of the contribution of each single constituent. This feature suggests that processed constituents in a composite could modify their individual water vapor sorption behavior. In addition, the interphase at the fiber/matrix interface could also intervene and create "a third compartment" with its own sorption properties, making the system more complex.

Modeling of Water Vapor Sorption Isotherms of WSF, PHBV, and Composites

GAB and Park models both fit all experimental sorption data (Table II), with satisfying R^2 (all higher than 0.99) and E (all below 8%) values, with however a slight better fit for the GAB model. From the GAB model, the first part of the isotherm was described essentially by the X_m and C_g parameters; the values obtained for the composite lay logically between the values of the individual constituents: PHBV and WSF. For the last part of the isotherm, the values of K for the composite were higher than the K of WSF and neat PHBV. As previously suggested with the rule of mixture, the sorption in the composites at high a_w was confirmed to be a "non-additivity" result of each individual constituent property.

For the Park model, the parameters A_L and b_L, representing specific hydrophilic groups able to absorb superficial water vapor molecules (first monolayer), were much lower for PHBV than WSF, indicating that the hydrophobic PHBV constituent did not have many specific sites for water vapor sorption as compared to the hydrophilic WSF constituent. As expected, the addition of WSF in PHBV resulted in an increase of these two parameters in PHBV/WSF composites, which, however still, remained lower than in the case of WSF alone. The parameter k_H, defined as the random adsorption by dissolution and diffusion of water molecules into the matrix, was higher in PHBV/WSF composites than in PHBV. Concerning the aggregate parameters, it was interesting to note that the K_a and n values, corresponding to the ability to form water clusters and the mean number of water molecules per water cluster respectively, were clearly increased by the incorporation of WSF particles in PHBV. For instance, the size of water vapor molecules aggregates followed the order: PHBV/20WSF (6.71) > PHBV/10WSF (5.03) > PHBV (3.26). Addition of increasing amounts of WSF modified the polymer properties (in agreement with decreasing crystallinity, Tm and Tc values, Table I) and caused interfacial gaps, both phenomena contributing to an increase in free volume and thus number and size of micro-voids available for water condensation. This was coherent with previous structural observations (occurrence of interfacial gaps at the fiber/matrix interface visible on light microscopic and SEM scans).[7] Consequently, composites showed a higher ability to condensate water (high k_H value) and to form water clusters (high K_a value) than PHBV and cluster size (n) tended to increase with WSF content.

To confirm this clustering effect, the Zimm and Lundberg[29] and ENSIC[41] theories have been used to determine the extent of

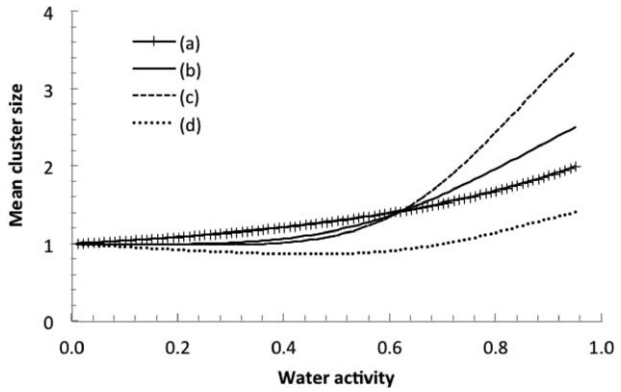

Figure 4. Application of the Zimm and Lundberg's theory [eq. (8)] to evaluate the mean cluster size of PHBV (a), PHBV/10WSF (b), PHBV/20WSF (c), and WSF (d) as function of the water vapor activity at 20°C.

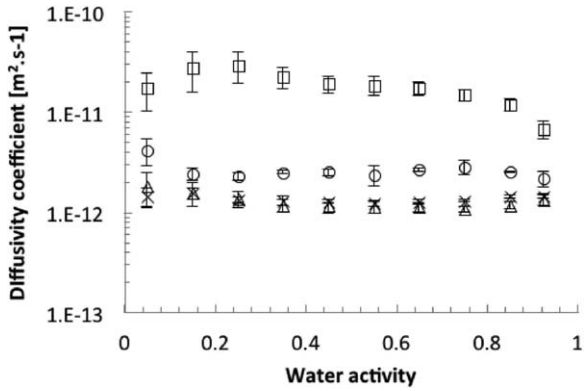

Figure 5. Effective water vapor diffusivity of PHBV (circle), PHBV/10WSF (cross), PHBV/20WSF (triangle), and WSF (square) identified with eq. (11).

water vapor clustering. From the Zimm and Lundberg's theory and according to Figure 4, significant water clustering started at a_w equal to zero in PHBV, at a water activity of 0.2 for PHBV/10WSF, 0.3 for PHBV/20WSF and 0.6 for WSF. At a water activity of 0.95, water vapor molecules aggregates size ranged in the following order: PHBV/20WSF (3.49) > PHBV/10WSF (2.50) > PHBV (1.99) > WSF (1.41). From the ENSIC theory and according to Table III, the value of the k_s representing the water–water interactions evolved in the following order: PHBV/20WSF (2.76) > PHBV/10WSF (1.88) > PHBV (1.66) > WSF (1.32). The results of both theories, developed under various and complex hypotheses representing the mean cluster size on the whole a_w range and the global water–water interactions, demonstrated that the water–water interaction extent in all materials was higher in the composites than in both individual constituents and corroborated the analysis made with the Park parameters.

Effective Water Vapor Diffusivity

According to Figure 5, D_{eff} could be considered as constant in PHBV and composites in the whole range of a_w. In WSF, D_{eff} first increased and then decreased slightly but significantly until an a_w of 0.3 and 0.95, respectively. This phenomenon was already observed by Gouanvé *et al.*,[40] in flax fibers and could be explained by a first increase of D_{eff} due to an increase of the molecular mobility and then a decrease due to the formation of water clusters in WSF whose size was large enough to behave similarly to bulk liquid water[42] at higher water activity. In our study, according to the Zimm and Lundberg theory, the mean cluster size in WSF increased slowly between a_w equal to 0.6 and 1; this trend could explain the slight decrease of D_{eff}.

Table III. ENSIC Fitting Parameters, Which Were Identified from the Water Vapor Sorption Isotherm of PHBV, WSF, and PHBV/WSF Composites at 20°C

	ENSIC parameters				
Sample	k_p	k_s	R^2	E	k_s/k_p
PHBV	0.002	1.661	0.995	6.98	705.69
WSF	0.104	1.321	0.991	9.08	12.64
PHBV/10WSF	0.007	1.880	0.994	5.92	260.15
PHBV/20WSF	0.009	2.759	0.988	13.26	299.48

D_{eff} in the WSF was lower than in other natural fiber species (Table IV). In all these previously published data, experimental diffusion was always obtained on an amount of numerous fibers, which could be as such, or shaped by different processes (compression, aqueous casting, and dry laying etc.). Whatever the method used, the sample always contains a significant amount of air, and is more representative of a mixture of air and fibers, than of fibers alone. Air with water diffusivity of 2.2×10^{-5} m^2 s^{-1} should favor the overall water transport and thus leads to an important overestimation of the apparent diffusivity through the contribution of the continuous gas phase.

Although D_{eff} was higher in WSF than PHBV, the addition of WSF in PHBV led to unexpectedly lower D_{eff} in composites. This result could be ascribed to (1) modification of the polymer matrix induced by WSF addition, (2) role of the interphase, and (3) modification of the fiber particle once embedded in the polymer. The impact of the addition fibers in polymer matrix property is usually ascribed to a modification of the matrix properties in the composite structure. In our study, the addition of WSF in PHBV matrix had a significant impact on the crystallinity rate and decreased Tc (Table I). Structural analysis also revealed the presence of an interphase that could increase the free volume and create micro-voids. However, these last two features were not in favor of a decrease of D_{eff} in composites.

Therefore, these unexpected effects of WSF on D_{eff} in composite should be, most likely, due to WSF structural change once the filler is embedded in the matrix. Hence, the identification of water vapor diffusivity on a piece of flat undamaged fiber wall and not on a single ground WSF might not reflect the same D_{eff} as in single milled WSF. Indeed as shown in Figure 6(a,b), the structure of a piece of WSF exhibits specific porous guide beams, such as phloem, xylem, and perivascular fibers, which could accelerate the diffusion of water vapor if compared to the structure of WSF obtained by successive grinding of native wheat straw, which was demonstrated to be less porous than native straw as revealed by evaluation of the porosity/density of

Table IV. Water Vapor Diffusivity Coefficients of Different Vegetal Fibers, Which Were Determined from Water Vapor Sorption Experiments Performed on Large Piles of Numerous Fibers (Data from the Literature). only the Last one (Present Study) was Obtained by Testing a Single Piece of Wheat Straw

Samples	Diffusivity coefficient ($\times 10^8$ m^2 s^{-1})	Experimental conditions	Environment	References
Sisal cellulosewhisker films	First half sorption $D_1 = 12.60$ Second half sorption $D_2 = 1.58$	Dynamic gravimetric water vapor sorption balance (DVS)	25°C, 80% RH	Belbekhouche *et al.*, (2011)[38] (from graphical lecture)
Sisal microfibrillated cellulose films	First half sorption $D_1 = 2.51$ Second half sorption $D_2 = 0.50$	ibid.	25°C, 80% RH	ibid.
Hemp fiber bundles	0.02	Gravimetric water vapor sorption in a climatic chamber	24°C, 80% RH	(Célino *et al.*, 2013[43]
Jute fiber bundles	0.04	ibid.	24°C, 80% RH	ibid.
Flax fiber bundles	0.02	ibid.	24°C, 80% RH	ibid.
Sisal fiber bundles	0.01	ibid.	24°C, 80% RH	ibid.
Agave fibers	First half sorption $D_1 = 0.46$ Second half sorption $D_2 = 2.24$	Dynamic gravimetric water vapor sorption balance (IGA)	25°C, 75% RH	(Bessadok *et al.*, 2009)[37]
	First half sorption $D_1 = 0.29$ Second half sorption $D_2 = 1.60$	ibid.	25°C, 84% RH	ibid.
Nonwovens flax fibers films	1.26	Dynamic gravimetric water vapor sorption (IGA)	25°C, 79% RH	(Gouanvé *et al.*, 2006)[40] (from graphical lecture)
Flax fiber fibers	First half sorption $D_1 = 79.40$ Second half sorption $D_2 = 179.00$	Dynamic gravimetric water vapor sorption balance (DVS)	25°C, 80% RH	(Alix *et al.*, 2009)[39] (from graphical lecture)
Wheat straw fiber films	0.00146 ± 0.00024	Dynamic gravimetric water vapor sorption (DVS)	20°C, 75% RH	This study
	0.00116 ± 0.00016	ibid.	20°C, 85% RH	ibid.

WSF after successive grinding of decreasing size.[34] Hence, D_{eff} in ground WSF dispersed in the PHBV polymer matrix could exhibit a lesser water vapor diffusivity coefficient and might be lower than D_{eff} in PHBV, or at least in neat PHBV. Note that D_{eff} in PHBV was also probably modified in composites due to the addition of fibers to an extent that was not quantifiable (increase or decrease of D_{eff} could be expected depending on polymer chains rearrangement and entanglements).

It can therefore be concluded that the experimental determination of water vapor diffusivity on a piece of flat WSF might still overestimate the D_{eff} of water vapor in the ground WSF when it is incorporated in the PHBV matrix. Hence, the only possibility to access the water vapor diffusion coefficient of the fibers embedded in the polymer matrix would be to identify the coefficient through a mass transfer modeling approach.

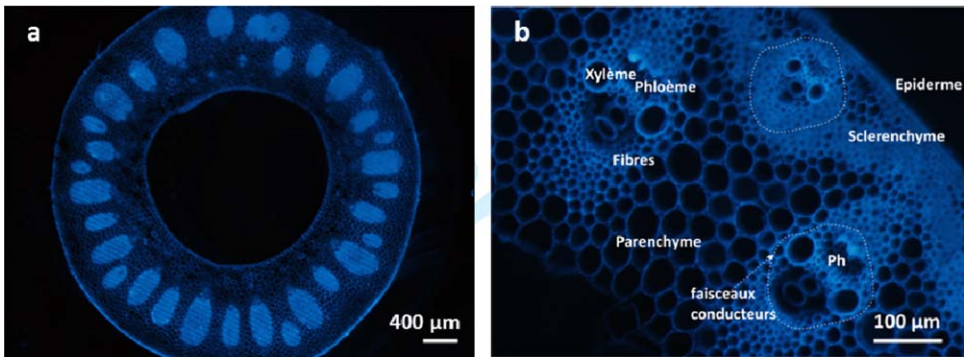

Figure 6. Fluorescence microscopy observation of a WSF node (3a) and internode (3b) cross sections. [Color figure can be viewed in the online issue, which is available at wileyonlinelibrary.com.]

CONCLUSIONS

Water vapor mass transfer properties of WSF, PHBV, and PHBV/WSF composites were investigated through the study of water vapor sorption and diffusion of these materials. From the water vapor sorption isotherm, the hydrophilic character of WSF was demonstrated to predominantly contribute to the water vapor sorption of the biocomposites, which presented a sigmoidal shape. Contribution of both PHBV and WSF to the composite water sorption isotherm did not follow the rule of mixture, revealing the existence of water vapor clustering and change in sorption properties of each individual constituent when blended in a composite structure. Based on Park, Zimm and Lundberg, and ENSIC theories, water clustering occurred in all materials to a higher extent in composite materials confirming the presence of some interfacial effects previously observed by SEM analysis. Concomitantly, although the water vapor diffusivity coefficient was higher in the WSF than in PHBV, incorporating WSF in PHBV always led to a decrease of D_{eff} in the composites. Considering the difficulty to experimentally determine D_{eff} in the ground WSF dispersed *in situ* in the PHBV matrix, D_{eff} was investigated on square pieces of WSF. The decrease of D_{eff} could be explained by the unavoidable structural differences between the square piece of straw and the ground one. In this perspective, future research studies should focus on a methodology to identify D_{eff} in single milled WSF dispersed in a PHBV polymer matrix through modeling approaches.

ACKNOWLEDGMENTS

This work was carried out in the framework of the EcoBioCAP project, which is supported by the European Commission through the Seventh Framework for Research & Technological Development (FP7/2011-2015) under the Grant Agreement FP7-265669.

REFERENCES

1. Mukherjee, T.; Kao, N. *J. Polym. Environ.* **2011**, *19*, 714.
2. Albuquerque, M. G. E.; Adiutori, R.; Trindade, N. M. P.; Carmo, I. T. D.; Oliveira, C. S. S.; Pardelha, F.; Reis, M. A. M. *Environ. Eng. Manag. J.* **2012**, *11*, 2012.
3. Carvalho, G.; Oehmen, A.; Albuquerque, M. G. E.; Reis, M. A. M. *N. Biotechnol.* **2014**, *31*, 257.
4. Duque, A. F.; Oliveira, C. S. S.; Carmo, I. T. D.; Gouveia, A. R.; Pardelha, F.; Ramos, A. M.; Reis, M. A. M. *N. Biotechnol.* **2014**, *31*, 276.
5. Berthet, M. A.; Angellier-Coussy, H.; Guillard, V.; Gontard, N. *J. Appl. Polym. Sci.* **2016**, *133*, DOI: 10.1002/app.42528.
6. Berthet, M. A.; Angellier-Coussy, H.; Machado, D.; Hilliou, L.; Staebler, A.; Vicente, A.; Gontard, N. *Ind. Crops Prod.* **2015**, *69*, 110.
7. Berthet, M. A.; Angellier-Coussy, H.; Chea, V.; Guillard, V.; Gastaldi, E.; Gontard, N. *Compos. A: Appl. Sci. Manuf.* **2015**, *72*, 139.
8. De Sales, J. A.; Patrício, P. S. O.; Machado, J. C.; Silva, G. G.; Windmöller, D. *J. Membr. Sci.* **2008**, *310*, 129.
9. Faruk, O.; Bledzki, A. K.; Fink, H. P.; Sain, M. *Prog. Polym. Sci.* **2012**, *37*, 1552.
10. Cho, S. W.; Gällstedt, M.; Hedenqvist, M. S. *J. Agric. Food Chem.* **2010**, *58*, 7344.
11. Mannberg, P.; Nyström, B.; Wallström, L.; Joffe, R. *J. Mater. Sci.* **2014**, *49*, 5265.
12. Srubar, W. V.; Billington, S. L. *Compos. A: Appl. Sci. Manuf.* **2013**, *50*, 81.
13. Sreekumar, P. A.; Albert, P.; Unnikrishnan, G.; Joseph, K.; Thomas, S. *J. Appl. Polym. Sci.* **2008**, *109*, 1547.
14. Marais, S.; Gouanvé, F.; Bonnesoeur, A.; Grenet, J.; Poncin-Epaillard, F.; Morvan, C.; Métayer, M. *Compos. A Appl. Sci. Manuf.* **2005**, *36*, 975.
15. Cagnon, T.; Méry, A.; Chalier, P.; Guillaume, C.; Gontard, N. *Innov. Food Sci. Emerg. Technol.* **2013**, *20*, 288.
16. Cagnon, T.; Guillaume, C.; Gastaldi, E.; Gontard, N. *J. Appl. Polym. Sci.* **2013**, *130*, 39509.
17. Guillaume, C.; Chalier, P.; Gontard, N. In Environmentally Compatible Food Packaging; Chiellini, E. Ed.; CRC Press: Boca Raton, **2008**; p 396.
18. Guillaume, C.; Guillard, V.; Gontard, N. In Advances in Fresh-Cut Fruits and Vegetables Processing; Martin-Belloso, O., Soliva-Fortuny, S., Eds.; CRC Press: Boca Raton, **2010**; p 255.
19. Guillaume, C.; Schwab, I.; Gastaldi, E.; Gontard, N. *Innov. Food Sci. Emerg. Technol.* **2010**, *11*, 690.
20. Corradini, E.; Ferreira, F. C.; Rosa, M. F. *Polímeros* **2014**, *23*, 807.
21. Martino, L.; Berthet, M. A.; Angellier-Coussy, H.; Gontard, N. *J. Appl. Polym. Sci.* **2015**, *132*, 41611.
22. Chea, V.; Angellier-Coussy, H.; Peyron, S.; Kemmer, D.; Gontard, N. *J. Appl. Polym. Sci.* **2016**, *133*(2), 41850.
23. Silva, G. G. D.; Couturier, M.; Berrin, J. G.; Buléon, A.; Rouau, X. *Bioresour. Technol.* **2012**, *103*, 192.
24. Avella, M.; La Rota, G.; Martuscelli, E.; Raimo, M.; Sadocco, P.; Elegir, G.; Riva, R. *J. Mater. Sci.* **2000**, *5*, 829.
25. Guillard, V.; Broyart, B.; Bonazzi, C.; Guilbert, S.; Gontard, N. *J. Food Sci.* **2003**, *68*, 555.
26. Al-Muhtaseb, A. H.; McMinn, W. A. M.; Magee, T. R. *J. Food Eng.* **2004**, *61*, 297.
27. Quirijns, E. J.; Van Boxtel, A. J. B.; Van Loon, W. K. P.; Van Straten, G. *J. Sci. Food Agric.* **2005**, *85*, 1805.
28. Lomauro, C. J.; Bakshi, A. S.; Labuza, T. P. *LWT Food Sci. Technol.* **1985**, *18*, 111.
29. Zimm, B. H.; Lundberg, J. L. *J. Phys. Chem.* **1956**, *60*, 425.
30. Favre, E.; Nguyen, Q. T.; Clément, R.; Néel, J. *J. Membr. Sci.* **1996**, *117*, 227.
31. Chivrac, F.; Angellier-Coussy, H.; Guillard, V.; Pollet, E.; Avérous, L. *Carbohydr. Polym.* **2010**, *82*, 128.
32. Guillard, V.; Chevillard, A.; Gastaldi, E.; Gontard, N.; Angellier-Coussy, H. *Eur. Polym. J.* **2013**, *49*, 1337.
33. Crank, J. The Mathematics of Diffusion, 2nd ed.; Oxford Science Publications: Oxford, UK, **1980**.

34. Montaño-Leyva, B.; Ghizzi D. da Silva, G.; Gastaldi, E.; Torres-Chávez, P.; Gontard, N.; Angellier-Coussy, H. *Ind. Crops Prod.* **2013**, *43*, 545.

35. Miguel, O.; Iruin, J. J. *J. Appl. Polym. Sci.* **1999**, *73*, 455.

36. Brunauer, S.; Deming, L. S.; Deming, W. E.; Teller, E. *J. Am. Chem. Soc.* **1940**, *62*, 1723.

37. Bessadok, a.; Roudesli, S.; Marais, S.; Follain, N.; Lebrun, L. *Compos. A Appl. Sci. Manuf.* **2009**, *40*, 184.

38. Belbekhouche, S.; Bras, J.; Siqueira, G.; Chappey, C.; Lebrun, L.; Khelifi, B.; Marais, S.; Dufresne, A. *Carbohydr. Polym.* **2011**, *83*, 1740.

39. Alix, S.; Philippe, E.; Bessadok, a.; Lebrun, L.; Morvan, C.; Marais, S. *Bioresour. Technol.* **2009**, *100*, 4742.

40. Gouanvé, F.; Marais, S.; Bessadok, a.; Langevin, D.; Morvan, C.; Métayer, M. *J. Appl. Polym. Sci.* **2006**, *101*, 23661.

41. Du, A.; Koo, D.; Theryo, G.; Hillmyer, M.; Cairncross, R. *J. Membr. Sci.* **2012**, *396*, 50.

42. Modesti, M.; Dall'Acqua, C.; Lorenzetti, a.; Florian, E. *J. Membr. Sci.* **2004**, *229*, 211.

43. Célino, A.; Fréour, S.; Jacquemin, F.; Casari, P. *J. Appl. Polym. Sci.* **2013**, *130*, 39148.